Robust and Practical 3D RFI Nulling for 5G and Radio Astronomy Coexistence

Siddharth Dongre, Tiep M. Hoang, Hanif Rahbari, and Alireza Vahid
Rochester Institute of Technology, Rochester, NY
Email: {sd4767, tmheme, hanif.rahbari, alireza.vahid}@rit.edu

***Abstract*—5G network operators are constantly under pressure from regulatory agencies who restrict the deployment of base stations (gNBs) close to incumbent services, such as radio astronomy services (RAS), to avoid interfering with them. Recent works for coexistence with RAS employ limited channel modeling approaches and use explicit out-of-band communication between the gNB and RAS. However, the strict latency requirements of 5G make explicit techniques less desirable due to their communication overheads. Deploying gNBs close to RAS is also not yet supported. In this paper, we propose a proactive implicit beamforming and interference nullification technique in which a gNB nullifies its downlink signal at a nearby RAS telescope while beamforming its users (UEs). We estimate the gNB-RAS channel using raytracing on open-source terrain maps which also accounts for the height of the gNB, UE and RAS telescope. We formulate a max-min rate problem for UEs under the constraint of maximum allowable interference power at the RAS and show that the time complexity of the max-min rate solution depends cubically on the number of gNB antennas. Hence, we propose a heuristic solution that achieves 4 orders of magnitude faster latency and 100 dBW lower interference power than the max-min rate solution with similar sum rate on users. Our proposed solution consistently achieves less than -310 dBW interference power in simulations, even when the gNB-RAS distance is less than 1 km, while being robust against channel estimation errors at more than 20 dB estimation SNR. Through over-the-air experiments, we demonstrate that our proposed scheme reduces the interference power to less than -115 dBW at the cost of 1-5 dB SNR loss at a nearby UE.**

***Index Terms*—5G, RAS, nullification, coexistence.**

I. Introduction

The demand for wireless bandwidth has been growing exponentially in recent years, driven by the increasing number of connected devices and the rising data consumption of users through applications such as ultra-high-definition media streaming, online gaming, and augmented and virtual reality [1]. This surge in demand is partly due to the accelerated deployment of 5G cellular networks. To meet the users' growing needs, 5G operators are striving for more efficient, smarter, and geographically widespread deployment of base stations (a.k.a. gNBs) to deliver ubiquitous, high data rate, and low-latency services [2], [3]. However, this rapid expansion is hindered by the scarcity of desirable wireless spectrum, which is becoming increasingly congested as more wireless services compete for frequencies, and by geographical limitations due to the presence of sensitive incumbent services.

Radio Astronomy Service (RAS) is one of the incumbents significantly affected by the proliferation of 5G networks. RAS uses highly sensitive radio telescopes that are easily disrupted by radio frequency interference (RFI), which makes it difficult to distinguish faint astronomical signals from the wireless signals generated by man-made transmissions. Aggressive 5G network expansion through emerging protocols such as 5G New Radio Unlicensed has led to a significant increase in RFI in the 5–7 GHz frequency bands which overlap with the 0–10 Ghz bands used by RAS telescopes [4]. Recognizing this potential conflict, regulatory bodies, such as the Federal Communications Commission (FCC) and the International Telecommunication Union (ITU), have set stringent limits to minimize RFI and protect RAS from harmful disruptions. For example, the ITU mandates an extremely strict regulation that any RFI on RAS ground stations needs to have less than -220 dBW interference power [5]. As a result, 5G operators are forced to place gNBs far away from RAS ground stations to limit the intensity of their RFI and avoid sanctions [6]. Due to these difficulties that both RAS and 5G networks have to face, there is a need to develop a fair and compliant spectrum sharing framework that allows 5G operators to coexist with RAS observatories effortlessly.

To embolden coexistence research, National Radio Dynamic Zones (NRDZs) have recently been proposed in the U.S. [7]. These zones employ large-scale testbeds to validate 5G and RAS coexistence schemes, as well as others such as satellite communications, in real-world setups. NRDZs work well with RAS telescopes that operate at almost 100% duty cycles across a wide range of frequencies, including 0–10 GHz. However, they require 5G operators to remain within interference threshold boundaries, especially for gNBs located close to the edges of the zones which pose a big challenge for the gNBs to meet user data rate requirements in that region [7]. Moreover, NRDZs do not yet cover observatories that only have access to small single-dish telescopes of less than 4 m diameter, such as the "KROC" telescope located in Ionia, NY, that is affected by gNBs within a 10 km radius [8]. To achieve the broader goal of NRDZs—establishing automated coexistence testing environments for all radio systems, there is a need to better protect smaller, less resourceful observatories. On this note, we argue that a more effective paradigm would be where gNBs could proactively nullify their interference at the location of the RAS observatories using highly scalable singular vector

The work of A. Vahid was in part supported by the National Science Foundation (NSF) grants CNS-2343964 and AST-2348589. Any opinions, findings, and conclusions or recommendations expressed in this material are those of the author(s) and do not necessarily reflect the views of the NSF.

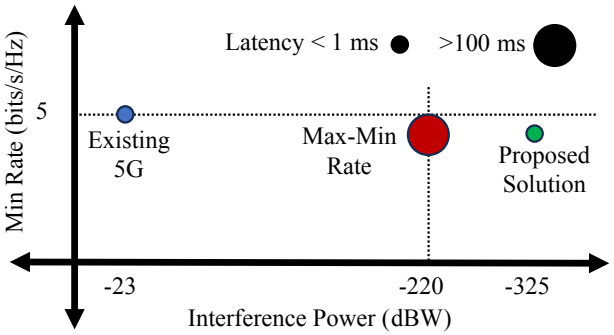

Fig. 1. Comparison of minimum rate versus interference power at RAS obtained by existing beamformers, the max-min rate solution and our proposed heuristic solution.

decomposition-based precoding techniques to overcome the challenge posed by being close to the observatories.

However, implementing such nullification schemes poses significant challenges: (1) gNBs need to coexist with passive RAS receivers that do not provide any *explicit* feedback for channel state information (CSI) carrying information about, for example, terrain reflections, (2) the nullifying precoder needs to minimize unintentional negative effects on 5G users (UEs) is minimized while nullification at the RAS should be sufficient enough to allow gNBs to be deployed close to them, and (3) computational complexity of the precoder needs to be low to satisfy strict latency requirements of 5G.

Existing works have attempted to address these challenges. A gNB may estimate the channel based on limited CSI feedback using techniques such as channel covariance matrices as features for deep learning frameworks [9] or estimating the angle of arrival and departure for deriving CSI [10]. However, these techniques are insufficient for modeling channels that also involve terrain reflections which significantly contribute to interference on RAS telescopes. To minimize the negative effects of nullification on UEs, interference broadcast channels using Gaussian-like interference channel models have been proposed, albeit with limited terrain reflection modelling [11]. Alternatively, explicit channel coordination schemes that avoid CSI exchange, such as sending stochastic characteristics via out-of-band links [4], [12] or using intelligent reflecting surfaces to mitigate RFI [13], face challenges in 5G due to their latency overhead and are undesirable for low-latency applications that require less than $0.5\,$ms latency [14]. Moreover, none of the works address all challenges fully while supporting gNBs within $1\,$km of RAS which is highly desirable for 5G.

To address these drawbacks, we proposed, in our preliminary work, the first entirely proactive and *implicit* nullification scheme that does not require any explicit CSI exchange between the gNB and RAS with support for the addition of external sensors to help with CSI estimation [15]. Our proposed coexistence mechanism addresses all the challenges (1)–(3) above and creates a win-win scenario for both 5G and RAS where 5G satisfies RFI limits on RAS, even when deploying the gNB close to the RAS telescope or NRDZ, while ensuring that any negative effect on UEs is minimized and the 5G latency requirements are satisfied. The idea is to nullify the gNB downlink signals at the location of the RAS telescope receiver using heuristically derived precoding schemes.

To benchmark our preliminary work, we formulated a max-min fair rate problem constrained by the $-220\,$dBW interference power limit at the RAS telescope. However, since the complexity of this problem scales cubically with the number of gNB antennas, we developed a novel heuristic precoding solution that leverages the gNB-RAS channel estimated using raytracing techniques over open-source terrain data [16] which incorporates latitude, longitude and heights of gNB, UEs and RAS. Our proposed scheme achieves a sum rate and minimum rate that is comparable to the max-min fair solution and existing default beamformers, while reducing the interference power to less than $-310\,$dBW, as shown in Fig. 1, satisfying RFI regulations. However, our preliminary work was limited since the robustness and practicality of our scheme in a real environment with imperfect CSI had not been investigated.

In this paper, we propose direct extensions to our preliminary work and experimentally demonstrate a robust and computationally light precoding scheme that performs significantly better than the state-of-the-art and minimizes loss in data rate for UEs, which is prevalent only in a small area around the RAS. The key contributions of this paper are as follows:

- We theoretically analyze the robustness of our scheme against imperfect estimation of the gNB-RAS and gNB-UE channels by deriving a general error bound on channel coefficients. By measuring the impact of erroneous channels on the interference power and the sum rate performance of our scheme, compared to the max-min rate solution, we demonstrate that our proposed scheme is robust against errors of variance less than 10^{-5}. Our proposed heuristic solution runs in $\mathcal{O}(M^2)$ time, which is faster than the max-min rate solution by a factor of KM for M gNB antennas and K UEs.
- We show that the minimum rate of our solution is similar to the max-min rate benchmark with $100\,$dBW lower interference power and 10^4 faster latency.
- We provide a radio environment map of the interference power in a $400\,\text{m} \times 400\,\text{m}$ area centered on the RAS telescope to show the precise nullification area of our proposed scheme which reduces the interference power in only a small region of $5\,$m radius around the RAS telescope and minimally affects the surrounding area.
- We experimentally evaluate our scheme by developing a proof-of-concept 5G and RAS coexistence testbed deployed using SDR devices. We demonstrate that our proposed scheme reduces the interference power to less than $-115\,$dBW, which is significant since we use SDRs that are much less sensitive than radio telescopes, at the cost of 1–5 dB SNR loss at a nearby UE. Our code and data is publicly available for reproducibility[1].

The rest of the paper is organized as follows. In Section II we provide a primer on RAS and raytracing for channel modeling. We then describe our open-loop beamforming and interference nullification technique in detail in Section III. The performance evaluation of our proposed technique is first provided in Section IV which covers simulation results and then in Section V which covers the experimental results. We

[1]https://github.com/nanosid/RAS-5G

TABLE I
LIST OF IMPORTANT ABBREVIATIONS.

Abbreviation	Description
CDL	Clustered Delay Line
CSI	Channel State Information
CSI-RS	CSI Reference Signal
gNB	Next Generation Evolved NodeB
NRDZ	New Radio Dynamic Zone
RAS	Radio Astronomy Services
RFI	Radio Frequency Interference
SBR	Shooting-and-Bouncing Rays
UE	User Equipment

then provide a review of related work in Section VI before concluding the paper in Section VII.

II. Background and System Model

We first provide an overview of RAS systems, followed by raytracing methods and a description of the 5G and RAS coexistence system model used in our paper. A list of important abbreviations used in this paper is provided in TABLE I.

A. 5G Precoding Techniques

In 5G networks, precoding techniques help improve spectral efficiency and system capacity while mitigating inter-user and inter-cell interference. Before sending a downlink message to a UE, the gNB needs to beamform its transmission to maximize the SINR at the receiving UE. To beamform on the UE, the gNB first transmits a CSI Reference Signal (CSI-RS) and then receives a CSI Feedback message from a UE containing the estimate of the CSI between them. Next, the gNB uses zero-forcing precoding, a type of linear precoding, to beamform on the UEs, where inter-user interference is mitigated by projecting the downlink signals of one user onto the null regions of the other users' channel vectors [14].

B. Radio Astronomy Services

Ground-based RAS stations observe deep space objects using low-frequency radio waves ranging from 0–10 GHz [17]. At these frequencies, RAS telescopes are looking for electron transitions in hydrogen atoms that can help locate distant celestial objects. These low-frequency radio waves, with wavelengths spanning from a few meters to several kilometers, can penetrate through dense clouds of gas and dust that obstruct visible light, enabling ground telescopes to observe celestial objects and phenomena that would otherwise remain concealed. Radio telescopes, designed to detect these radio waves, are typically situated in remote locations to minimize RFI from external sources, such as gNBs, and keep the interference power of RFI sources below -220 dBW at the RAS telescope [5].

C. Raytracing Methods

The shooting-and-bouncing rays (SBR) method of raytracing is used to determine the propagation paths of the downlink signal between the gNB and the RAS telescope. This method involves backtracking by generating rays from the intended receiver, in this case, the RAS telescope, and tracing the rays as they reflect or "bounce" off of objects and terrain in the environment. After backtracking, the rays that reach the transmitter, in this case, the gNB, are the propagation paths of the downlink signal. The total number of possible propagation paths is controlled by manually assigning a maximum number of ray reflections which limits the number of bounces a ray will make before it reaches the gNB. A ray that has undergone path loss of greater than -130 dB before it reaches the receiver is considered to be terminated. Note that, although the RAS is sensitive to rays as weak as -220 dB, it is reasonable to assume a -130 dB limit for channel estimation purposes since weaker rays inevitably get dominated by the stronger ones and, hence, don't make a significant impact on the channel coefficient between the gNB and RAS.

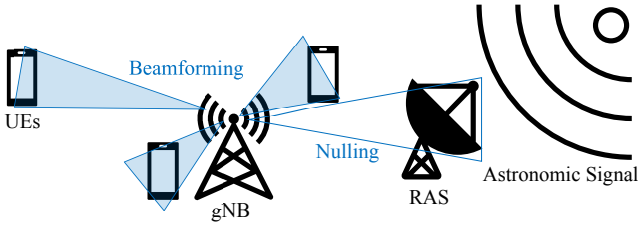

Fig. 2. 5G and RAS coexistence system model.

D. Clustered Delay Line (CDL) Channel Model

The CDL channel model, defined in 3GPP specifications [18], is suited for MISO/MIMO systems with frequencies ranging from 0.5 GHz to 100 GHz and a maximum bandwidth of 2 GHz. This makes it a perfect choice for our 5G and RAS coexistence system. The CDL channel model considers clusters of multipath channel components between the gNB and a UE or RAS. Each cluster consists of several rays with unique path loss, path delay and AoA/AoD parameters that are obtained from the raytracing method described above. It uses the Rayleigh channel distribution when there is no line-of-sight component, and the Rician distribution otherwise. The channel coefficients for Rayleigh and Rician models are given by,

$$\text{Rayleigh} : \mathbf{h} = \sum_{c=1}^{C}\sum_{r=1}^{R_c} \alpha_{c,r} e^{j\phi_{c,r}}, \tag{1}$$

$$\text{Rician} : \mathbf{h} = \sqrt{\frac{K}{K+1}} h_{LOS} + \sqrt{\frac{1}{K+1}} \sum_{c=1}^{C}\sum_{r=1}^{R_c} \alpha_{c,r} e^{j\phi_{c,r}} \tag{2}$$

where, C is the number of clusters, R_c is the number of rays in the c-th cluster, K is the Rician-K factor, $\alpha_{c,r}$ and $\phi_{c,r}$ is the magnitude and phase of the r-th ray in the c-th cluster, respectively [18]. Now, $\alpha_{c,r} = \sqrt{P_{c,r}}$, where $P_{c,r}$ is the power of the (c,r)-th ray. Finally, $P_{c,r} = P_{gNB} - L_{c,r}$ where P_{gNB} is the transmit power of the gNB and $L_{c,r}$ is the path loss of the (c,r)-th ray across the distance $d_{c,r}$ travelled by the ray from position p_{gNB} to either p_{UE} or p_{RAS}.

E. System Model

An illustration of the system model can be seen in Fig. 2. In our 5G and RAS coexistence system, we only assume one gNB. We argue that, for inter-cell scenarios with multiple gNBs, our proposed scheme can be independently implemented on each gNB separately to nullify its respective downlink signal on the RAS telescope without the need to coordinate with other gNBs. As a result, even in the presence of multiple interfering gNBs, the aggregate interference power at the RAS remains below the -220 dBW requirement. This is because the presence of downlink signals from other gNBs does not impact our singular-value decomposition-based heuristic precoding scheme that we develop in the following section. We assume the gNB has M omnidirectional dipole antennas serving K UEs. All UEs are less than 100 m away from the gNB. The gNB transmits on carrier frequency f_c within the FR1 frequency bands of up to 7.125 GHz. We consider a single-dish telescope that is 2 m high and between 100 m and 12 km away from the gNB with one parabolic antenna operating in the $0-10$ GHz range. The CSI between the gNB and the kth UE is denoted by $\mathbf{h}_k$ and that between the gNB and RAS is denoted by $\mathbf{h}_{gR}$. Note that $\mathbf{h}_k$ and $\mathbf{h}_{gR}$ are time-variant, but we omit the dependency on time since the channels are updated after each 1 ms 5G subframe when the gNB executes channel estimation. Finally, we argue that nullifying the interference due to uplink transmissions from UEs is out of the scope of this work since it is a significantly challenging problem on its own that we intend to investigate and solve in future work.

III. Open-loop Beamforming and Interference Nullification

In this section, we first develop a problem formulation to maximize the minimum rate for UEs under an interference power constraint at the RAS. We then describe our raytracing approach to estimate the gNB-RAS channel, followed by our highly efficient heuristic solution to achieve our objective. A reference list for the important notation used in the following sections is given in TABLE II.

A. Problem Formulation

We primarily consider RFI from the downlink signal of one gNB. Hence, the signal $r_R(t)$ received by the RAS telescope is given by,

$$r_R(t) = m_s(t) + \mathbf{h}_{gR}\mathbf{w}^{\mathbf{H}} m_g(t) + n_R(t) \tag{3}$$

where $m_s(t)$ is the astronomical signal, $m_g(t)$ is the RFI from the gNB, $\mathbf{h}_{gR} \in \mathbb{C}^{1\times M}$ is the channel between the gNB and the receiver of the RAS telescope, $\mathbf{w} \in \mathbb{C}^{1\times M}$ is the precoding scheme applied at the gNB, and $n_R(t)$ is the receiver noise at the RAS telescope. Similarly, the downlink signal received by the kth UE is given by

$$r_k(t) = \mathbf{h}_k\mathbf{w}^{\mathbf{H}} m_g(t) + n_k(t) \tag{4}$$

where $\mathbf{h}_k \in \mathbb{C}^{1\times M}$ is the channel between the gNB and the kth UE, $m_g(t)$ is the gNB downlink signal, and $n_k(t)$ is the receiver noise at the kth UE. In (3) and (4) we assume the channels $\mathbf{h}_{gR}$ and $\mathbf{h}_k, \forall\, k = 1, ..., K$, are time-invariant for the entire 1 ms duration of a 5G subframe (contained in $m_g(t)$). However, $\mathbf{h}_k$ is updated after each subframe when the gNB performs channel estimation for its UEs while $\mathbf{h}_{gR}$ remains constant.

TABLE II
List of Important Mathematical Notations.

Notation	Description
$\mathbf{w}$	Downlink precoding matrix at gNB
M	Number of antennas at gNB
K	Number of UEs
R	Maximum number of ray reflections
f_c	Carrier frequency
$r_R(t)$	Signal received by the RAS telescope
$m_s(t)$	Astronomical signal being measured by the RAS telescope
$m_g(t)$	Downlink RFI from gNB
$n_R(t)$	Receiver noise at the RAS telescope
$\mathbf{h}_{gR}$	Channel between the gNB and RAS telescope
$r_k(t)$	Signal received by the kth UE
$n_k(t)$	Receiver noise at the kth UE
$\mathbf{h}_k$	Channel between the gNB and the kth UE
ρ_g	Transmit power of the gNB
σ_k^2	Expected power of the receiver noise of the kth UE
ϵ	Maximum allowable interference power at RAS
$\mathbf{P}$	Null space of the gNB-RAS channel
$\sigma^2_{\mathbf{h}_{gR}}$	Variance of errors in gNB-RAS channel
$\sigma^2_{\mathbf{h}_k}$	Variance of errors in the gNB-kth UE channel

We assume that the gNB operates based on a quality-of-service (QoS) criteria [14], which is typically formulated using a max-min fair rate problem [19]. More precisely, the gNB aims at maximizing the minimum rate achieved by all UEs as captured by the problem shown below:

$$\max_{\mathbf{w}\in\mathbb{C}^{1\times M}} \min_{k\in\{1,\ldots,K\}} \frac{\mathbb{E}(|\mathbf{h}_k\mathbf{w}^{\mathbf{H}} m_g(t)|^2)}{\mathbb{E}(|n_k(t)|^2)} \tag{P1}$$

$$\mathbf{s.t.}\ \frac{\mathbb{E}(|m_s(t)|^2)}{\mathbb{E}(|\mathbf{h}_{gR}\mathbf{w}^{\mathbf{H}} m_g(t) + n_R(t)|^2)} \geq \mu \tag{5}$$

$$0 < \|\mathbf{w}\|^2 \leq \rho_b \tag{6}$$

where μ is the minimum SINR threshold for the RAS telescope, and ρ_b is the beamforming power budget of the gNB. The problem (P1) is challenging to solve due to the non-convexity of the objective function in (P1) and constraint in (5). To simplify it, we first rewrite the expectation ($\mathbb{E}$) terms inside (P1), as shown below:

$$\mathbb{E}(|\mathbf{h}_k\mathbf{w}^{\mathbf{H}} m_g(t)|^2) = \rho_g|\mathbf{h}_k\mathbf{w}^{\mathbf{H}}|^2 \tag{7}$$

$$\mathbb{E}(|n_k(t)|^2) = \sigma_k^2 \tag{8}$$

where ρ_g is the baseband signal power of the gNB downlink signal, $m_g(t)$, and σ_k^2 is the expected power of the receiver noise of the kth UE. We assume that the terms $m_s(t)$ and $n_R(t)$ are significantly dependent on parameters such as the distance of the astronomical object, observation integration time, the aperture size of the telescope and the temperature of the receiver. Due to the complexity of defining these parameters, we instead consider the equivalent constraint of a maximum allowable interference power ϵ of the gNB downlink signal at the RAS telescope. We also assume that the noise

power σ_k^2 of each of the K UEs and the baseband signal power ρ_g remains constant. Hence, we rewrite the problem as shown below:

$$\max_{\mathbf{w}\in\mathbb{C}^{1\times M}} \min_{k\in\{1,...,K\}} |\mathbf{h}_k\mathbf{w}^{\mathbf{H}}|^2 \tag{P2}$$

$$\text{s.t. } |\mathbf{h}_{gR}\mathbf{w}^{\mathbf{H}}|^2 \leq \epsilon,\ \epsilon > 0 \tag{9}$$

$$0 < \|\mathbf{w}\|^2 \leq \rho_b. \tag{10}$$

The problem in (P2) is similar to a Max-Min fair beamforming problem, such as the one in [19] with the added maximum allowable interference constraint, which is solvable in polynomial time after it is transformed using the Semidefinite Relaxation method as shown below:

$$\max_{\mathbf{W}\in\mathbb{C}^{M\times M}} \min_{k\in\{1,...,K\}} \mathbf{Tr}(\mathbf{H}_k\mathbf{W}) \tag{P3}$$

$$\text{s.t. } \mathbf{Tr}(\mathbf{H}_{gR}\mathbf{W}) \leq \epsilon,\ \epsilon > 0 \tag{11}$$

$$0 < \mathbf{Tr}(\mathbf{W}) \leq \rho_b, \mathbf{W} \succeq 0 \tag{12}$$

where $\mathbf{W} = \mathbf{w}^{\mathbf{H}}\mathbf{w}, \mathbf{H}_k = \mathbf{h}_k{}^{\mathbf{H}}\mathbf{h}_k, \mathbf{H}_{gR} = \mathbf{h}_{gR}{}^{\mathbf{H}}\mathbf{h}_{gR}$.. Note that we have dropped the $\text{rank}(\mathbf{W}) = 1$ constraint to relax (P3) into a semidefinite program and $\mathbf{W} \succeq 0$ denotes that the matrix $\mathbf{W}$ is positive semidefinite. We can further introduce an auxiliary variable τ and remove the minimization problem in (P3) while also converting the outer maximization problem into a minimization one as shown below:

$$\min_{\mathbf{W}\in\mathbb{C}^{M\times M},\tau\in\mathbb{R}} -\tau \tag{P4}$$

$$\text{s.t. } \mathbf{Tr}(\mathbf{H}_k\mathbf{W}) \geq \tau,\quad \forall k \in \{1,...,K\} \tag{13}$$

$$\mathbf{Tr}(\mathbf{H}_{gR}\mathbf{W}) \leq \epsilon,\quad \epsilon > 0 \tag{14}$$

$$0 < \mathbf{Tr}(\mathbf{W}) \leq \rho_b,\quad \mathbf{W} \succeq 0 \tag{15}$$

The problem in (P4) is solvable because it involves minimizing a convex objective function with convex constraints. Due to the impracticality of deriving a closed-form solution to (P4), we use analytical solvers, such as CVX, a package for specifying and solving convex optimization problems [20], [21]. However, the worst-case time complexity of (P4) is $\mathcal{O}(KM^3)$, which is still significant for $M \approx K$. Hence, in the following sections, we develop a heuristic solution with lower computational complexity and nullification at the RAS telescope, and a comparable sum rate for the UEs, while addressing challenges such as estimating the $\mathbf{h}_{gR}$ channel without channel feedback.

B. Coarse Estimation of $\mathbf{h}_{gR}$

To estimate $\mathbf{h}_{gR} \in \mathbb{C}^{1\times M}$, we need the path delays, the path gains, and the angles of arrival and departure (azimuth and zenith directions) for all the signal propagation paths originating at the M antennas of the gNB and terminating at the RAS telescope's receiver. The SBR raytracing method (see Section II-C) is used to populate these path parameters for each signal path from each of the M antennas. For this, only the geographical locations of the gNB and RAS are needed, along with access to open-source terrain maps like OpenStreetMap. The locations of the gNB and RAS are initialized in the terrain maps and the terrain data is used to evaluate rays between the gNB and RAS, assuming R maximum number of ray reflections. These rays involve reflections from the ground and nearby buildings, if any. Once the rays have been evaluated, path parameters from these rays can be extracted using the `raytrace()` function of MATLAB's Communication Toolbox.

The extracted path parameters can then be used to create an NR CDL channel model delay profile which can then provide a coarse channel estimate for $\mathbf{h}_{gR}$, using the `nrCDLChannel()` channel object of MATLAB's 5G Toolbox based on 5G specifications [18]. Although this channel estimate is not dynamic, it provides a coarse estimate sufficient for nullifying the gNB downlink signal at the RAS. This is because the primary components (due to line-of-sight) of this coarse channel estimate dominate other components (for example, due to reflections) by at least one order of magnitude.

C. Heuristic Solution to Nullify The gNB Signal at RAS

We assume the gNB uses linear precoding, such as the zero-forcing precoding technique to nullify the gNB interference at points of interest by projecting the downlink signal onto the null space of those points [14]. Similarly, we define the precoding scheme $\mathbf{w}_{null} \in \mathbb{C}^{1\times M}$, which only nullifies the gNB downlink signal at the RAS but does not simultaneously beamform on the UEs. Let $\mathbf{P}$ denote the orthonormal basis for the null space of the $\mathbf{h}_{gR}$ channel. Hence, $\mathbf{h}_{gR}\mathbf{P}\mathbf{P}^{\mathbf{H}} = \mathbf{0}$. When the precoding vector $\mathbf{w}_{null}$ is a member of the subspace $\mathbf{P}$ and is applied to the gNB downlink signal, it will ensure that the signal's null region overlaps with the location of the RAS telescope. Hence, we define $\mathbf{w}_{null}$ as,

$$\mathbf{w}_{null} = c\mathbf{v}_{gR}\mathbf{P}\mathbf{P}^{\mathbf{H}} \tag{16}$$

where $\mathbf{v}_{gR} \in \mathbb{C}^{1\times M}$ contains the singular vectors of the $\mathbf{h}_{gR}$ channel and c is any scalar. By combining (3) and (16), we can see that the downlink signal x is nullified since $\mathbf{P}$ is in the null space of $\mathbf{h}_{gR}$ and $\mathbf{h}_{gR}\mathbf{w}^{\mathbf{H}}{}_{null} = \mathbf{h}_{gR}\mathbf{P}\mathbf{P}^{\mathbf{H}}\mathbf{v}^{\mathbf{H}}{}_{gR} = \mathbf{0}$. Hence, the precoding scheme $\mathbf{w}_{null}$ will perfectly nullify the gNB at the RAS, however, it may also harm some of the UEs. Because there are no constraints on $\mathbf{w}_{null}$, it may inadvertently nullify locations where there is no RAS telescope and may even nullify some UEs. Hence, we slightly modify (16) as shown below,

$$\mathbf{w}_{heu} = c\mathbf{v}_{gU}\mathbf{P}\mathbf{P}^{\mathbf{H}} \tag{17}$$

where $\mathbf{v}_{gU} \in \mathbb{C}^{1\times M}$ contains the singular vectors of the channel matrix $\mathbf{H}_{gU} = [\mathbf{h}_1^{\mathbf{T}}; \mathbf{h}_2^{\mathbf{T}}; ...; \mathbf{h}_K^{\mathbf{T}}]$ containing the channel vectors to all the K UEs. The expression for $\mathbf{w}_{heu}$ in (17) satisfies the constraint in (9) since $\mathbf{h}_{gR}\mathbf{P}\mathbf{P}^{\mathbf{H}} = \mathbf{0}$, and hence is a valid solution for (P4). Although not an optimal solution, the worst-case time complexity of our proposed solution $\mathbf{w}_{heu}$ in (17) is $\mathcal{O}(M^2)$, which is better than the max-min rate solution from problem (P4) by a factor of KM when using analytical solvers.

D. Proposed Beamforming Algorithm

The algorithm for our proposed beamformer is listed in **Algorithm 1**. To calculate the gNB-RAS channel $\mathbf{h}_{gR}$, we require the geographic coordinates, in latitude and longitude,

and height of the gNB and the RAS which are stored in the variables $gNBSite$ and $RASSite$, respectively. We then use MATLAB's `raytrace()` method that takes the $gNBSite$ and $RASSite$ objects as input and determines the rays of propagation paths between the gNB and RAS as output in $RASrays$. This is followed by the `nrCDLChannel()` method that takes the $RASrays$ object as input and returns the channel estimate of the gNB-RAS channel in $\mathbf{h}_{gR}$. Although this operation is computationally intensive, with time complexity $\mathcal{O}(NR)$ where N is the number of rays spawned [22], it only needs to be performed occasionally, for example, when the gNB-RAS channel needs to be calibrated based on RFI reports from the RAS. Note that the complexity can be controlled by tuning N and R, for example, we use $R = 3$ in our simulations and experiments since rays with more reflection are weak and have a negligible effect on the $\mathbf{h}_{gR}$ channel. Next, we use the `nrChannelEst()` method that takes the CSI Feedback of the kth UE stored in $rCSI(k)$ and the known CSI-RS indices stored in $CSIRS$ to obtain the channel estimate $\mathbf{H}_{gU}(k)$ of the channel between the gNB and the kth UE. The time complexity of the `nrChannelEst()` method is $\mathcal{O}(MK)$ and is executed before sending every 5G frame. Next, we obtain the singular vectors $\mathbf{v}_{gU}$ of the channel matrix for all UEs $\mathbf{H}_{gU}$, followed by the orthonormal basis of the null space of the $\mathbf{h}_{gR}$ channel which is stored in $\mathbf{P}$. Finally, we obtain our proposed beamformer $\mathbf{w}_{heu}$ using $\mathbf{v}_{gU}$ and $\mathbf{P}$ as per (17). The last three operations each have a time complexity of $\mathcal{O}(M^2)$ and are executed for each 5G frame. Hence, for $K \approx M$, the overall time complexity of our proposed beamforming algorithm is $\mathcal{O}(M^2)$ or $\mathcal{O}(K^2)$. The parameters used in our algorithm take $\mathcal{O}(M^2)$ locations to store in memory. Hence, the space complexity is also $\mathcal{O}(M^2)$. This is comparable to existing precoding methods such as those that use singular-value decomposition. Hence, the power consumption requirements of our scheme are also comparable to existing gNB deployments. Note that the power consumption on UEs and RAS remains unaffected since our scheme does not require any changes to their existing operations.

Algorithm 1 Proposed Beamforming Algorithm

$gNBSite \leftarrow$ gNB Coordinates, Height
$RASSite \leftarrow$ RAS Coordinates, Height
$RASrays \leftarrow$ `raytrace`($gNBSite$, $RASSite$)
$\mathbf{h}_{gR} \leftarrow$ `nrCDLChannel`($RASrays$)
$k \leftarrow 1$
for $k \leq K$ **do**
  $CSIRS \leftarrow$ CSI-RS Indices
  $rCSI(k) \leftarrow$ Received CSI Feedback
  $\mathbf{H}_{gU}(k) \leftarrow$ `nrChannelEst`($rCSI(k), CSIRS$)
  $k \leftarrow k + 1$
end for
$\mathbf{v}_{gU} \leftarrow$ `svd`($\mathbf{H}_{gU}$)
$\mathbf{P} \leftarrow$ `null`($\mathbf{h}_{gR}$)
$\mathbf{w}_{heu} \leftarrow \mathbf{v}_{gU}\mathbf{P}\mathbf{P}^{\mathbf{H}}$

E. Channel Estimation Error

In our 5G and RAS coexistence system, channel estimation errors can occur in two ways: (1) error in estimating the channel $\mathbf{h}_k$ between the gNB and the Kth UE due to highly dynamic time-varying channels or due to receiver noise, and (2) error in deriving the channel $\mathbf{h}_{gR}$ between the gNB and the RAS due to inaccurate modeling of terrain reflections in ray tracing methods. We model the channel estimation error in $\mathbf{h}_k$ and $\mathbf{h}_{gR}$ separately, along with its effect on the interference power at the RAS and the sum rate on the UEs. Next, we establish a general error bound for the Rayleigh and Rician channel distributions.

1) Error in $\mathbf{h}_k$: We use the 5G channel estimation procedure to estimate the $\mathbf{h}_k$ channel in every 1 ms 5G frame transmitted by the gNB to the kth UE. Assuming that the channel coherence time is greater than 1 ms, we argue that channel estimation error in $\mathbf{h}_k$ occurs primarily due to noise at the kth UE's receiver. Due to noise, let $\hat{\mathbf{h}}_k$ be the inaccurate channel given by,

$$\hat{\mathbf{h}}_k = \frac{\mathbf{r}_{CRS(k)} + \mathbf{n}_k}{\mathbf{b}_{CRS}} \tag{18}$$

where $\mathbf{r}_{CRS(k)}$ is the CSI-RS signal received by the kth UE, $\mathbf{b}_{CRS}$ contains the CSI-RS reference symbols sent by the gNB, and $\mathbf{n}_k \sim \mathcal{CN}(\mu_{\mathbf{h}_k}, \sigma^2_{\mathbf{h}_k})$ is complex normal noise with mean $\mu_{\mathbf{h}_k}$ and variance $\sigma^2_{\mathbf{h}_k}$.

Assuming that noise affects all K UEs independently, we denote the inaccurate channel matrix $\hat{\mathbf{H}}_{gU} = [\hat{\mathbf{h}}_1^{\mathbf{T}}; \hat{\mathbf{h}}_2^{\mathbf{T}}; ...; \hat{\mathbf{h}}_K^{\mathbf{T}}]$ containing the inaccurate channels for all K UEs. The singular vectors of $\hat{\mathbf{H}}_{gU}$ are then derived using singular vector decomposition (SVD) to obtain $\hat{\mathbf{v}}_{gU}$, which is then used to obtain the inaccurate heuristic solution given by,

$$\hat{\mathbf{w}}_{hk} = c\hat{\mathbf{v}}_{gU}\mathbf{P}\mathbf{P}^{\mathbf{H}} \tag{19}$$

Due to the errors in the beamformer $\hat{\mathbf{w}}_{hk}$, the sum rate on the K UEs will be affected. This change in sum rate is given by,

$$\Delta SR_{hk} = SR(\hat{\mathbf{w}}_{hk}) - SR(\mathbf{w}_{heu}) \tag{20}$$

where $SR(\mathbf{w})$ denotes the sum rate of the K UEs when using beamformer $\mathbf{w}$. Similarly, the change in interference power is given by,

$$\Delta IP_{hk} = IP(\hat{\mathbf{w}}_{hk}) - IP(\mathbf{w}_{heu}) \tag{21}$$

where $IP(\mathbf{w}) = 10\log_{10}(|\mathbf{h}_{gR}\mathbf{w}^{\mathbf{H}}|^2)$ is the interference power of the gNB at the RAS when using beamformer $\mathbf{w}$.

2) Error in $\mathbf{h}_{gR}$: When using ray tracing methods to obtain the channel between the gNB and the RAS, there will likely be inaccuracies in modeling terrain reflections. These terrain reflection inaccuracies are manifested in the form of errors in AoA and AoD estimates, path gains, and path delays. These errors can be modeled by complex normal perturbations $\mathbf{n}_{gR} \sim \mathcal{CN}(\mu_{\mathbf{h}_{gR}}, \sigma^2_{\mathbf{h}_{gR}})$ which leads to an inaccurate channel estimate $\hat{\mathbf{h}}_{gR}$ given by,

$$\hat{\mathbf{h}}_{gR} = \mathbf{h}_{gR} + \mathbf{n}_{gR} \tag{22}$$

We then obtain $\hat{\mathbf{P}} = \texttt{null}(\hat{\mathbf{h}}_{gR})$ which is the orthonormal basis of the null space of the inaccurate channel estimate $\hat{\mathbf{h}}_{gR}$. Next, we obtain the inaccurate beamformer $\hat{\mathbf{w}}_{hgR} =$

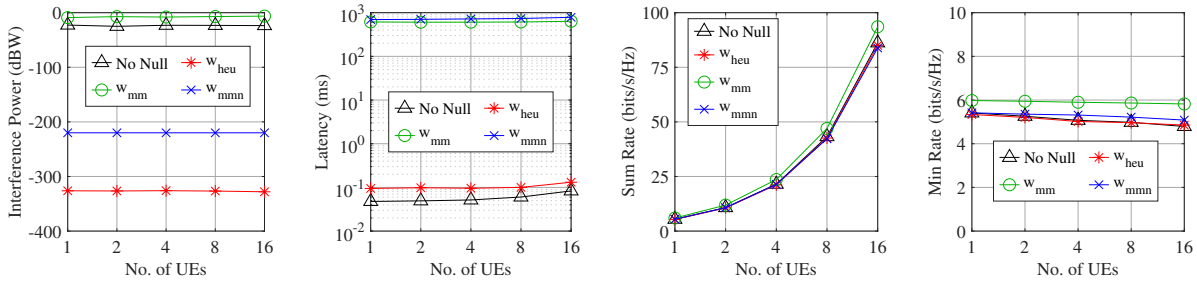

(a) Nullification. (b) Latency. (c) Sum rate. (d) Minimum rate.

Fig. 3. Comparing the interference power, latency, sum rate and minimum rate for the max-min rate solution $\mathbf{w}_{mmn}$ (w/ RAS null), $\mathbf{w}_{mm}$ (w/o RAS null), and our heuristic $\mathbf{w}_{heu}$ for K UEs.

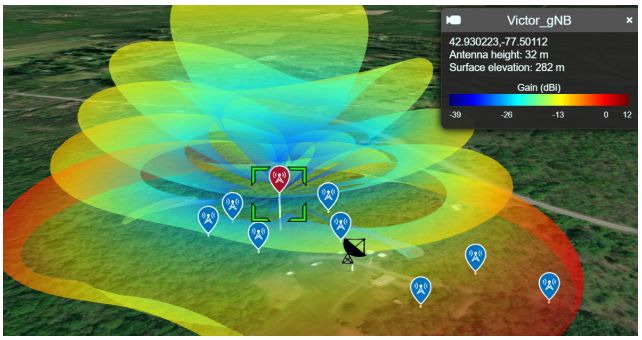

Fig. 4. Radiation pattern of the gNB when using our heuristic solution. The red pin indicates the location of the simulated gNB, the black telescope is the RAS, and the remaining blue pins are the locations of simulated UEs.

$c\mathbf{v}_{gU}\hat{\mathbf{P}}\hat{\mathbf{P}}^{\mathbf{H}}$, which is used to evaluate changes in sum rate ΔSR_{hgR} and interference power ΔIP_{hgR} similar to (20) and (21), respectively.

3) General Error Bound: The variance of the channel estimation error can be used to provide a measure of the error bounds of the channel coefficients. Let $\hat{\mathbf{h}} = \mathbf{h} + e$ denote the erroneous channel, where $e \sim \mathcal{CN}(0, \sigma_e^2)$. Hence, from (1) and (2), the error bounds considering Rayleigh and Rician distributions are given by,

$$\text{Rayleigh} : \sigma^2_{\hat{\mathbf{h}}} = \sum_{c=1}^{C}\sum_{r=1}^{R_c} \sigma^2_{\alpha_{c,r}} + \sigma_e^2 \tag{23}$$

$$\text{Rician} : \sigma^2_{\hat{\mathbf{h}}} = \frac{K}{K+1}\sigma^2_{h_{LOS}} + \frac{1}{K+1}\sum_{c=1}^{C}\sum_{r=1}^{R_c} \sigma^2_{\alpha_{c,r}} + \sigma_e^2 \tag{24}$$

where $\sigma^2_{(.)}$ denotes variance, $\sigma^2_{\alpha_{c,r}} = P_{gNB} - L_{c,r}$ is the variance of the magnitude of the (c,r)-th ray, P_{gNB} is the transmit power of the gNB and $L_{c,r}$ is the path loss across the (c,r)-th ray [18].

IV. Performance Evaluation

In this section, we compare our heuristic solution with the optimal one, then measure the change in gNB interference power at the RAS telescope, the change in SNR for a moving UE, and the latency of our beamforming algorithm.

A. MATLAB Simulation Setup

We evaluate the performance of our beamforming algorithm by running simulations in MATLAB on an 8-core CPU with parallel processing capabilities. We implement the coarse channel estimation technique described in Section III-B using the `raytrace()` and `nrCDLChannel()` objects of MATLAB, as explained in Section III-B. We assume $R = 1, 2, 3$ maximum number of ray reflections. To estimate the channels between the gNB and the K UEs, we implement CSI-RS and CSI Feedback messages sent by the gNB and UEs respectively. The gNB can have $M = \{4, 8, 16\}$ antennas transmitting at $f_c = \{0.7$ GHz, 1.8 GHz, 5.9 GHz$\}$ carrier frequencies, and supporting $K = \{1, 2, 4, 8, 16\}$ UEs. The distance between the gNB and the RAS telescope varies between 100 m, and 12 km. We run $10,000$ unique iterations for each combination of gNB-RAS distance, M, f_c, K, and R for an extensive performance evaluation. Our simulations assume a real RAS observatory, "KROC" [8], located at the Max Farash Center for Observational Astronomy in Ionia, NY. We define this RAS telescope in all our MATLAB simulations, which remains constant, and randomize gNBs and UEs at simulated locations around it. In Fig. 4, we show the radiation pattern of our proposed heuristic solution $\mathbf{w}_{heu}$ for one of the simulation runs, where the red pin indicates the location of the simulated gNB, less than 1 km from the RAS telescope (the highlighted blue pin), and the remaining blue pins are the locations of simulated UEs. We can see that our proposed solution $\mathbf{w}_{heu}$ nullifies at the location of the RAS telescope, while also achieving a sum rate comparable to the optimum.

B. Max-Min Rate versus Heuristic Solutions

To prove the effectiveness of our proposed heuristic solution, we compare, (a) the beamformer used by gNBs in practice which does not nullify the RAS telescope by default, denoted by "No Null", (b) our proposed heuristic solution $\mathbf{w}_{heu}$, (c) the solution to problem (P4), denoted by $\mathbf{w}_{mmn}$, and (d) the solution to problem (P4) but without the RAS interference limit constraint in (14), denoted by $\mathbf{w}_{mm}$. We set $M = 16$, $f_c = 1.8$ GHz, $R = 3$ and $K = \{1, 2, 4, 8, 16\}$.

In Fig. 3 (a), we can see that the interference power achieved by $\mathbf{w}_{heu}$ is more than 100 dBW lower than $\mathbf{w}_{mmn}$. This is because $\mathbf{w}_{heu}$ is in the null space of $\mathbf{h}_{gR}$, bringing $|\mathbf{h}_{gR}\mathbf{w}^{\mathbf{H}}|^2$, which controls the interference power at the RAS, very close to zero. Additionally, as seen in Fig. 3 (c), the sum rate

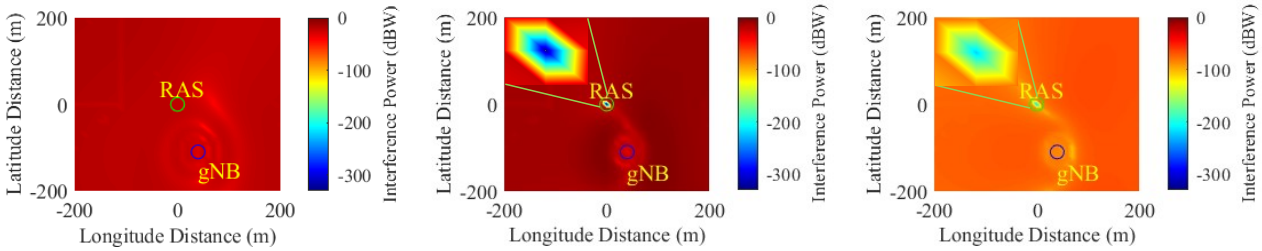

(a) No Nullification. (b) Heuristic Solution $\mathbf{w}_{heu}$. (c) Max-min rate solution $\mathbf{w}_{mmn}$.

Fig. 5. Radio environment maps showing the level of interference power in a $400 \times 400\,\mathrm{m}^2$ area centered at the location of the RAS telescope receiver when using the $\mathbf{w}_{heu}$ and $\mathbf{w}_{mmn}$ solutions. The RAS and gNB sites are highlighted in green and blue circles, respectively. The top right of $\mathbf{w}_{heu}$ and $\mathbf{w}_{mmn}$ solutions shows a zoomed-in $20 \times 20\,\mathrm{m}^2$ area around the RAS.

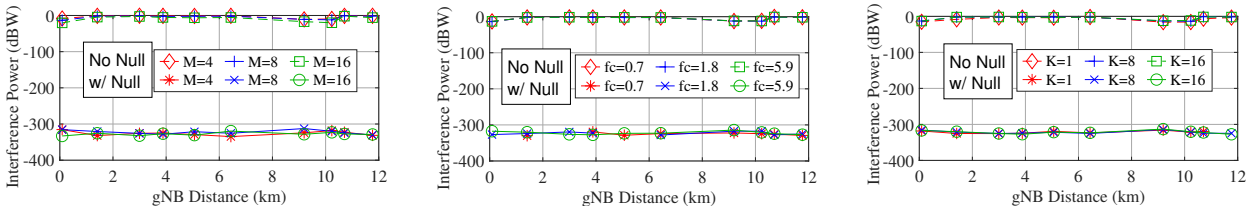

(a) $f_c = 5.9$ GHz, $R = 3$, $K = 16$. (b) $M = 16$, $R = 3$, $K = 16$. (c) $M = 16$, $f_c = 5.9\,\mathrm{GHz}$, $R = 3$.

Fig. 6. Interference power of the gNB at the RAS telescope with and without nullification, plotted in solid and dashed lines, respectively, while varying the gNB-RAS distance and the parameters M, f_c and K.

for both $\mathbf{w}_{heu}$ and $\mathbf{w}_{mmn}$ is comparable to when there is no nullification being performed. This shows that both $\mathbf{w}_{heu}$ and $\mathbf{w}_{mmn}$ are acceptable solutions for 5G networks as the effect on UEs is not significant. Note that the sum rate when performing no nullification ("No Null") is indeed less than $\mathbf{w}_{mm}$ since in practice gNBs use a closed-form solution based on singular value decomposition of the UE channels, instead of a slower, optimal one due to strict latency constraints [14]. In fact, as seen in Fig. 3 (b), the latency of $\mathbf{w}_{heu}$ is consistently less than $0.5\,\mathrm{ms}$, while that of $\mathbf{w}_{mmn}$ and $\mathbf{w}_{mm}$ is nearly $1000\,\mathrm{ms}$, 4 orders of magnitude higher, which shows that our proposed solution $\mathbf{w}_{heu}$ is evaluated significantly faster. Note that the $0.5\,\mathrm{ms}$ latency requirement of 5G includes frame transmission time as well [14], and since our scheme takes less than $0.5\,\mathrm{ms}$ we get more available time for the frames to be transmitted from the gNB to the UEs. Moreover, as seen in Fig. 3 (d), the minimum rate achieved by the UEs is practically the same when comparing $\mathbf{w}_{heu}$ to the default "No Null" beamformer while decreasing by less than $1\,\mathrm{bits/s/Hz}$ when comparing to $\mathbf{w}_{mm}$. Note that $\mathbf{w}_{heu}$ and $\mathbf{w}_{mmn}$ achieve practically the same minimum rate, which shows that our heuristic solution achieves results close to the max-min rate solution of problem (P4).

In Fig. 5, we compare the radio environment maps illustrating the interference power around a $400 \times 400\,\mathrm{m}^2$ area centered at the RAS telescope receiver, $5\,\mathrm{m}$ in height, when using the default "No Null" beamformer in Fig. 5 (a), the $\mathbf{w}_{heu}$ solution in Fig. 5 (b), and the $\mathbf{w}_{mmn}$ solution in Fig. 5 (c). We can see that the $\mathbf{w}_{heu}$ and $\mathbf{w}_{mmn}$ solutions significantly reduce the interference power but only in a small region around the location of the RAS telescope receiver while other locations remain largely unaffected. The affected region can be approximated by a circle of radius $5\,\mathrm{m}$. This shows that UEs will remain unaffected by the RAS nullifying beamformers $\mathbf{w}_{heu}$ and $\mathbf{w}_{mmn}$ as long as they are outside this $5\,\mathrm{m}$ circle. We can consider this to be an acceptable compromise since most radio observatories do not allow the use of external radio devices around their premises. We also tested a special case of the $\mathbf{w}_{mmn}$ solution where we set the RAS interference limit constraint to $-326\,\mathrm{dBW}$, to match the interference power achieved by our proposed $\mathbf{w}_{heu}$ solution. In this case, we observe that the sum rate and minimum rate of the $\mathbf{w}_{mmn}$ solution approaches zero for $K = 16$ UEs. Considering these results, we argue that our proposed heuristic solution $\mathbf{w}_{heu}$ is more practical and effective than the max-min rate solution $\mathbf{w}_{mmn}$ and hence we use only $\mathbf{w}_{heu}$ to evaluate the following results.

C. Interference Power

We measure the interference power of the gNB downlink signal at the RAS telescope to verify if $\mathbf{w}_{heu}$ satisfies the constraint in (14). In Fig. 6, we plot the interference power of the gNB at the RAS telescope versus increasing gNB-RAS distance and M to show their effect on the performance of our scheme. The interference power when using the default precoding scheme that the gNB applies to achieve near optimum sum rate at its UEs, without nullifying the RAS, is plotted using dashed lines and our $\mathbf{w}_{heu}$ precoding scheme that also simultaneously nullifies the gNB signal at the RAS telescope is plotted using solid lines. Our proposed solution incurs at most $-300\,\mathrm{dBW}$ interference power at the RAS telescope for all gNB-RAS distances, while it varies between -350 – $-310\,\mathrm{dBW}$ for varying M, f_c and K. In our set of simulations, with the gNB is less than $1\,\mathrm{km}$ away, the interference power was the worst at $-312\,\mathrm{dBW}$ for $M = 8$ antennas, $f_c = 5.9\,\mathrm{GHz}$, $R = 3$ ray reflections and $K = 16$ UEs. This shows that our scheme meets the RAS interference constraint in (14) for most practical cases of gNB-RAS distance and M. Additionally,

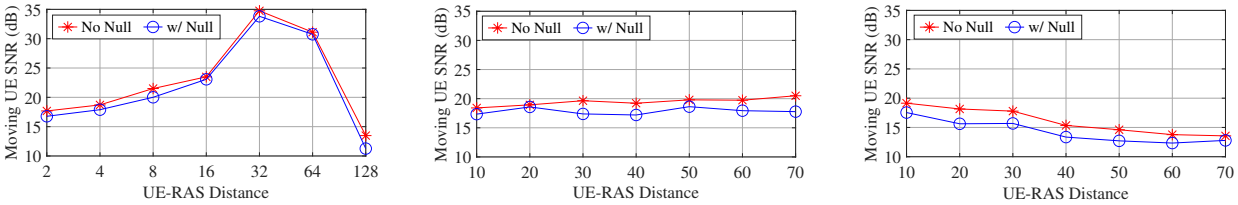

(a) Case 1. (b) Case 2. (c) Case 3.

Fig. 7. SNR at a single moving UE that starts at the RAS telescope location and increases its height, longitude and latitude.

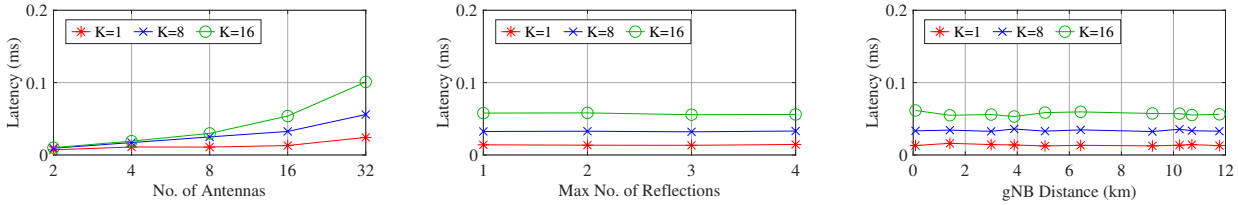

(a) Dist.$=1\,$km, $f_c = 5.9\,$GHz, $R = 3$. (b) Dist.$=1\,$km, $M = 16$, $f_c = 7\,$GHz. (c) $M = 16$, $f_c = 2.4\,$GHz, $R = 3$.

Fig. 8. Latency of our scheme while varying the parameters M, R, K, and the gNB-RAS distance.

our nullification scheme performs well even in an edge case with $K = 8$ UEs surrounding the RAS telescope in a circle with $1\,$m radius, where the interference power is observed to be -333 dBW, with a total sum rate of $28\,$bits/s/Hz, compared to no nullification getting -37 dBW interference power and $36\,$bits/s/Hz sum rate. To test the generalization of our proposed scheme, we measured the effect of antenna array configurations on the interference power at the RAS telescope. We tested for $M = 16$ antennas arranged in $1 \times 16, 2 \times 8$ and 4×4 configurations and observed that the impact on the interference power is negligible. We argue that this is due to the distance between the gNB and RAS telescope being much larger than the inter-antenna separation.

D. Effect of a moving UE

In Fig. 7, we plot the SNR at a moving UE to analyze the impact of changing the height and location of UEs on our scheme. We test three cases of movement: (1) UE moves vertically $2, 4, 8, ..., 128\,$m, above the RAS telescope (2) UE moves eastward (increasing longitude) at increments of $10\,$m, and (3) UE moves northward (increasing latitude) at increments of $10\,$m. In all three cases, the UE starts at the same latitude and longitude as the RAS telescope. Firstly, we note that in all three cases, the difference in SNR with and without our nullification scheme in use is within 2–3 dB. This shows that our scheme incurs only a small loss in QoS of the UEs when they move around the RAS. In case 1, we see that the SNR of the UE increases as it moves vertically, since the UE is actually getting closer to the gNB that is at $30\,$m height, after which the SNR starts decreasing again. In case 2, the SNR remains fairly constant since the increasing longitude does not create a significant change in the distance to the gNB (as seen in Fig. 5). However, in case 3, the UE moves away from the gNB as it increases latitude, thus causing a decrease in SNR.

E. Latency

To show that our proposed scheme satisfies the latency requirements of 5G, in Fig. 8, we plot the latency of our proposed beamforming and interference nullification algorithm, where we observe that the latency is within $0.5\,$ms for all the gNB operating parameters that we tested. Latency is measured by observing the current system time before and after executing the equation (17). In Fig. 8 (a), we observe that the latency of our proposed scheme increases with M and K for constant gNB-RAS distance of $1\,$km, $f_c = 5.9\,$GHz, and $R = 3$, since M and K are the dimensions of the channel matrix $\mathbf{H}_{gU}$ directly controlling the computational complexity of our algorithm. Although our proposed scheme takes more than $0.5\,$ms for $K = 16$ UEs and $M = 32$ antennas, we argue that gNBs with a higher number of antennas also have faster processing capabilities, better than the 8-core CPU used in our simulations, which would likely reduce the latency below $0.5\,$ms. We hope to test the latency of our scheme on such high-performing gNBs in future work. In Fig. 8 (b), we observe that the latency is unaffected by the maximum number of ray reflections, R, for constant gNB-RAS distance of $1\,$km, $M = 16$ and $f_c = 7\,$GHz. This is because the ray tracing algorithm used to determine a coarse estimate of the gNB-RAS channel, $\mathbf{h}_{gR}$, needs to be run only once. Once the gNB has the $\mathbf{h}_{gR}$ channel, it can use the same channel object for all subsequent precoder computations, unless there are significant changes in the terrain and environment between the gNB and RAS. Hence, it does not affect the latency of our scheme. Finally, in Fig. 8 (c), we see that the latency of our proposed scheme is mostly unaffected when increasing the gNB-RAS distance for constant $M = 16$, $f_c = 2.4\,$GHz, and $R = 3$.

F. Channel Estimation Error

To test the robustness of our scheme against erroneous channels, as prefaced in III-E, we plot the interference power due to errors in the gNB-RAS and gNB-UE channels for $M = 16$ antennas and $K = 8$ UEs. First, in Fig. 9 (a), we plot the impact on interference power due to errors in the gNB-RAS channel. The solid lines represent no error and the dashed lines represent the erroneous channel. We observe that errors in the gNB-RAS channel severely impact

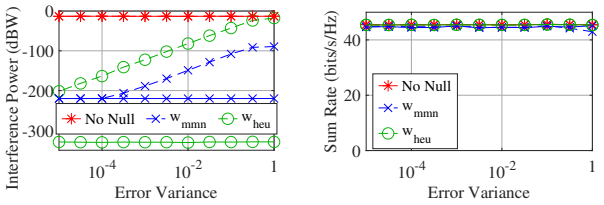

(a) Interference Power at RAS. (b) Sum rate of users.

Fig. 9. Impact of errors in the gNB-RAS channel, plotted in dashed lines, on the interference power and sum rate when using the max-min rate solution $\mathbf{w}_{mmn}$ and our heuristic solution $\mathbf{w}_{heu}$ versus error variance with $M = 16$ antennas, $f_c = 5.9\,\text{GHz}$, $K = 8$ UEs.

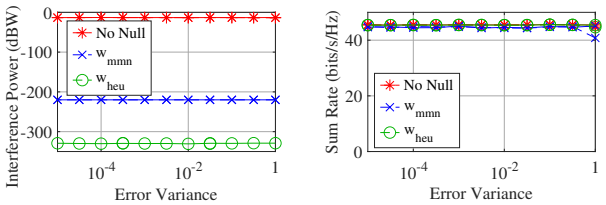

(a) Interference power at RAS. (b) Sum rate of users.

Fig. 10. Impact of errors in the gNB-UE channels, plotted in dashed lines, on the interference power and sum rate when using the max-min rate solution $\mathbf{w}_{mmn}$ and our heuristic solution $\mathbf{w}_{heu}$ versus error variance with $M = 16$ antennas, $f_c = 5.9\,\text{GHz}$, $K = 8$ UEs.

the interference power at the RAS which is now 120–300 dBW higher when using the proposed heuristic solution $\mathbf{w}_{heu}$, for error variance ranging from 10^{-5} to 1. The max-min rate solution with RAS null $\mathbf{w}_{mmn}$ is also impacted and it now gets 0–130 dBW higher interference power. We observe that our heuristic solution is more sensitive to errors in the gNB-RAS channel than the max-min rate solution. This is due to our heuristic solution nullifying a single point in space, the receiver of the RAS telescope, which is the result of using the null space of the gNB-RAS channel in the $\mathbf{w}_{heu}$ solution. We argue that, although the channel approximations across the area of the telescope are similar, nullifying over the entire area removes the strong dependency on the single point at the RAS receiver. To address this issue, we plan on improving our proposed heuristic beamformer in future work where we nullify a region/volume of space around the telescope receivers, instead of a single point. Note that the sensitivity to errors does not affect the performance of our scheme even when deployed in hilly or urban terrain. We also observe that the sum rate of the UEs is almost completely unaffected by errors in the gNB-RAS channel, as shown in Fig. 9 (b), which is expected behavior since errors in the gNB-RAS channel do not affect the beamforming done using gNB-UE channels. Because interference power is more sensitive to errors when using $\mathbf{w}_{heu}$, the max-min rate solution $\mathbf{w}_{mmn}$ is better at handling errors in the gNB-RAS channel.

In Fig. 10 (a), we see that the interference power at the RAS is almost unaffected due to errors in the gNB-UE, for both the max-min rate solution and our heuristic solution. This is expected behavior since the errors in the gNB-UE channels do not affect the null space of the gNB-RAS channel. The impact on the sum rate of $K = 8$ UEs due to errors in gNB-UE channels is shown in Fig. 10 (b). We observe that the sum rate decreases by 5 bits/s/Hz when using the max-min rate solution $\mathbf{w}_{mmn}$ but only when the error variance is 1. For other values of error variance, the impact on sum rate is negligible for both solutions. This shows that our proposed heuristic solution $\mathbf{w}_{heu}$ is more robust against errors in the gNB-UE channels, compared to the max-min rate solution.

V. Experimental Evaluation

To test the feasibility and performance of our proposed beamforming scheme on real radio devices, we developed a proof-of-concept 5G and RAS coexistence testbed using software-defined radios USRP X310 [23] and USRP B210 [24]. In Fig. 11, we see the setup of a transmitter site as the gNB, denoted by the red pin, and two receiver sites as the RAS and UE, denoted by the blue pins, respectively. Rays of propagation paths that reflect only once have been plotted and rays with more reflections have been omitted for illustrative purposes. To obtain 3D models of the buildings in the given area, we use OpenStreetMap and import it in MATLAB so that the `raytracing()` method correctly models ray propagation and reflections over the buildings and terrain between the gNB and RAS. In Fig. 12, we see the location of the USRP X310 as the gNB inside the GCI lab, and the USRP B210 RAS outside. The same B210 is later used to measure downlink SNR at the UE, by moving the cart carrying the B210 1 m in the West direction. A list of all experimental parameters is provided in TABLE III. In this setup, we configure the center frequency $f_c = 5.35\,\text{GHz}$, which was at the time an idle channel. The transmit power of the X310 is 10 dBm, using two 2 dBi dipole antennas, and the receiving B210 with one 2 dBi dipole antenna is set to the maximum receiver gain of 76 dB due to the high path loss between the X310 and B210. In our current testbed, we only have access to USRPs with a maximum of two transmit antennas which is why we only use one UE and one RAS since the gNB X310 will be unable to nullify on one RAS and beamform on more than one UE with only two antennas. We validated this small-scale setup in MATLAB simulations where we achieved less than -220 dBW interference power at the RAS.

TABLE III
List of important experimental parameters.

Parameter	Value	Parameter	Value
gNB antennas	2	Center frequency	5.35 GHz
gNB Tx power	12 dBm	Channel Bandwidth	10 MHz
RAS/UE Rx Gain	76 dB	gNB-RAS distance	10,15,20 m
Baseline Rx Power	-120 dBW	RAS-UE distance	1 m
No. of UEs	1	Max No. of Ref (R)	3

In Fig. 13, we compare the performance of $\mathbf{w}_{mmn}$ and $\mathbf{w}_{heu}$ the interference power at the RAS B210 and downlink SNR at the UE B210 when gNB-RAS distance is $10, 15, 20$ m. We observe that $\mathbf{w}_{heu}$ achieves 4–12 dBW lower interference power, but also 1–7 dB lower SNR when compared to $\mathbf{w}_{mmn}$.

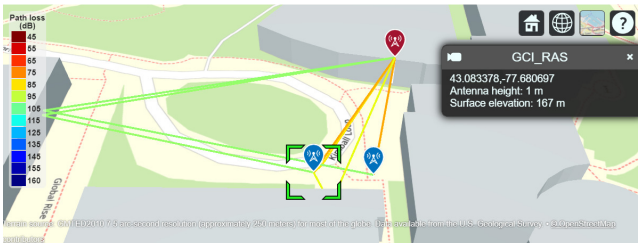

Fig. 11. Setup of gNB, RAS and UE sites around the GCI lab in MATLAB, showing rays of propagation paths that reflect only once (for illustration), which is used to determine the gNB-RAS channel.

(a) Inside GCI lab. (b) Outside GCI lab.

Fig. 12. Hardware setup of the gNB and RAS inside and outside the GCI building.

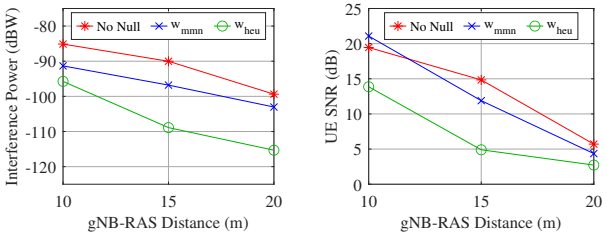

(a) Interference Power at RAS. (b) Downlink SNR at UE.

Fig. 13. Interference power at an RAS telescope and sum rate at a UE when using USRP B210s as the receivers.

Note that the baseline received power measured on the RAS B210, when the gNB X310 is not transmitting, was -120 dBW. The high received power is due to a 76 dB receiver gain applied at the receiving B210 for both UE and RAS. This is done to account for the low transmit power of the gNB X310 which is 10 mW. However, if the receiver gain was 0 dB, the baseline received power would be -196 dBW, and the interference power achieved by our proposed beamformer would be -171 dBW when the gNB is 10 m away from the RAS and -191 dBW when the gNB is 20 m away. Note that due to measurement limitations and imperfections in our USRP B210, we are unable to measure the interference power of signals lower than the -220 dBW ITU requirement. However, when using a noise factor to model these imperfections in small-scale simulations, we achieve results similar to our real experiments. These results show that, although not perfect, the proof-of-concept hardware implementation of our proposed beamformer achieves the goal of reducing the interference power at the RAS and yields promising results. In the future, we plan on developing a more sophisticated hardware testbed with more UEs and a gNB with at least $M = 8$ antennas and deploying it near a real radio telescope with much more sensitive receivers through collaborations with a radio observatory.

VI. Related Work

In this section, we briefly summarize related works that have proposed methods for RAS protection zones, spectrum band management and RFI cancellation. TABLE IV compares our proposed work with these existing methods from the perspective of the key features of our work: (1) low latency, (2) CSI Feedback requirement, (3) low computational complexity, and (4) minimal effect on UE QoS.

A. RAS Protection Zones

A dynamic protection zone is proposed in [25] in which the authors created a framework to measure instantaneous equivalent power flux density and derived a threshold for it beyond which RFI from satellites is detrimental to radio telescopes. Through simulations, they show that current transmission masks for RFI are insufficient for radio telescopes that operate and have much higher sensitivity for the detection of weak astronomical objects. Similar measurements studies have been performed, such as the one in [26] in which the authors developed a software-defined-radio-based testbed at the Hat Creek Radio Observatory to model and characterize the RF environment and flag ground and drone-based RFI sources. Their experiments show the potential danger of RFI and the need for the protection of RAS stations.

B. Spectrum Band Management

A reactive spectrum sharing scheme is proposed in [27] which supervises levels of interference coming from cellular base stations at the sensitive receiver sites and applies an exponentially weighted moving average to determine spectrum allocation decisions with the help of a zone management system. The POWDER [28] wireless testbed is used to deploy real coexistence scenarios to evaluate this scheme using over-the-air experiments and show high spectrum utilization at the RDZ with lower interference periods at the sensitive receivers. Another spectrum sharing paradigm is proposed in [29] in which the authors analyze the impact of RFI coming from satellite communication systems onto RAS ground telescopes and demonstrate how existing RFI mitigation techniques can be used to protect RAS. The proposed spectrum sharing paradigm for the coexistence of RAS telescopes and satellite systems involves the reorganization of spectrum bands to minimize emission in RAS-allocated spectrum bands and beamforming approaches to suppress RFI from satellites which reduces the sample loss rate at the telescopes. However, these spectrum sharing schemes support coexistence in either time, frequency or space at a time, but not all three simultaneously which is a key feature of our work.

C. RFI Cancellation

A signal cancellation scheme is proposed in [30] in which the authors develop and blueprint a reconfigurable intelligent

TABLE IV
COMPARISON OF RELATED WORK.

Related Work	Features			
	Latency (ms)	CSI Rqrmt	Time Complexity	Low Effect on UE QoS
[24][25]	$\sim 10^4$	✓	$\mathcal{O}(K^2)$	✓
[26][27][28]	$\sim 10^5$	✓	$\mathcal{O}(K^2)$	✓
[29][30]	$\sim 10^4$	✓	$\mathcal{O}(K^2)$	✓
Our Work	$\sim 10^{-1}$	✗	$\mathcal{O}(K^2)$	✓

surface design that cancels RFI from ground-based sources, such as cellular base stations, at the RAS telescopes by controlling the phase and amplitude of radio waves and redirecting them in 3D space. Through simulations, they show improvement in RFI cancellation performance when compared to a uniform rectangular array. Another low-overhead interference cancellation scheme is proposed in [31] in which the authors develop a compression network and mapping network model for RFI coming from LTE base stations that first compresses complex baseband RFI into a smaller latent space and then maps it to the RFI observed at the telescope, effectively reducing the communication overhead and computation complexity compared to existing methods while maintaining RFI mitigation quality. However, these schemes rely on out-of-band communication links between the passive receivers and active sources of RFI which is not a necessity in our work.

VII. CONCLUSION AND FUTURE WORK

In this paper, we have developed a proactive and open-loop beamforming and interference nullification scheme to facilitate 5G and RAS coexistence. We have formulated a problem to maximize the minimum rate for UEs under an interference power constraint of -220 dBW at the RAS telescope. We then propose a highly efficient heuristic solution, based on singular vector decomposition, whose time complexity is better by a factor of KM. We have also shown that our proposed solution has a similar sum rate and minimum rate for UEs when compared to existing default beamformers and the max-min solution while achieving more than 100 dBW lower interference power at the RAS and a latency that is 4 orders of magnitude faster than the max-min solution. Through extensive simulations we have shown that our proposed solution consistently achieves less than -310 dBW interference power at the RAS, even when the gNB is less than 1 km from the RAS telescope, and is robust against moving UEs that vary their location and elevation. We have shown that our proposed scheme is robust against erroneous channel for error variance less than 10^{-5} and proved that our proposed heuristic solution evaluates in $\mathcal{O}(M^2)$ time complexity. Through experiments, we have demonstrated that our proposed scheme reduces the interference power to less than -115 dBW at the cost of 1–5 dB SNR loss at a nearby UE. For future work, we plan on improving our heuristic solution to nullify the entire surface of the RAS telescope antenna and improve the robustness of our technique against errors in channel estimation and open-source terrain data.

REFERENCES

[1] E. Ekudden. (2021, Oct.) Exponential capability grouth. exponential potential - ericsson. [Online]. Available: https://tinyurl.com/3wu7924d

[2] D. Qiu, M. Lavergne, A. Samba, H. Afifi, and Y. Gourhant, "Machine learning for estimating the impact of adding new mobile network cells," in *IEEE Global Commun. Conf.*, Dec. 2023, pp. 6109–6114.

[3] M. Filo, C. H. Foh, S. Vahid, and R. Tafazolli, "Performance analysis of ultra-dense networks with regularly deployed base stations," *IEEE Trans. Wireless Commun.*, vol. 19, no. 5, pp. 3530–3545, May 2020.

[4] S. Chakraborty, G. Hellbourg, M. Careem, D. Saha, and A. Dutta, "Collaboration with cellular networks for RFI cancellation at radio telescope," *IEEE Trans. on Cogn. Commun. Netw.*, vol. 9, no. 3, pp. 765–778, Jun. 2023.

[5] International Telecommunications Union Radiocommunication Sector (ITU-R). (2003) Recommendation ITU-R RA.769. [Online]. Available: https://tinyurl.com/3kdjuxe5

[6] FCC Enforcement Bureau. (2020) Enforcement overview. [Online]. Available: https://tinyurl.com/mux57ppz

[7] M. Zheleva, C. R. Anderson, M. Aksoy, J. T. Johnson, H. Affinnih, and C. G. DePree, "Radio dynamic zones: Motivations, challenges, and opportunities to catalyze spectrum coexistence," *IEEE Commun. Mag.*, vol. 61, no. 6, pp. 156–162, Jun. 2023.

[8] M. Pepe. (2020) ART - autonomous radio telescope - ASRAS. [Online]. Available: https://tinyurl.com/yarn7a47

[9] A. M. Elbir, "A deep learning framework for hybrid beamforming without instantaneous CSI feedback," *IEEE Trans. Veh. Technol.*, vol. 69, no. 10, pp. 11 743–11 755, Oct. 2020.

[10] P. N. Alevizos, X. Fu, N. D. Sidiropoulos, Y. Yang, and A. Bletsas, "Limited feedback channel estimation in massive MIMO with non-uniform directional dictionaries," *IEEE Trans. Signal Process.*, vol. 66, no. 19, pp. 5127–5141, Oct. 2018.

[11] M. Zohdy, A. Tajer, and S. Shamai, "Distributed interference management: A broadcast approach," *IEEE Trans. Commun.*, vol. 69, no. 1, pp. 149–163, Jan. 2021.

[12] M. Careem, S. Chakaraborty, A. Dutta, D. Saha, and G. Hellbourg, "Spectrum sharing via collaborative RFI cancellation for radio astronomy," in *IEEE Int. Symp. Dynamic Spectr. Access Netw.*, Dec. 2021, pp. 97–104.

[13] Z. Zou, X. Wei, D. Saha, A. Dutta, and G. Hellbourg, "SCISRS: Signal cancellation using intelligent surfaces for radio astronomy services," in *IEEE Global Commun. Conf.*, Dec. 2022, pp. 4238–4243.

[14] *Physical layer procedures for data*, 3GPP Technical Specification 38.214, Jul. 2020.

[15] S. Dongre, T. M. Hoang, H. Rahbari, and A. Vahid, "Low-latency RFI nulling and multi-user scaling for 5G and radio astronomy coexistence," in *IEEE Consumer Communications & Networking Conference*, Las Vegas, USA, Jan. 2025.

[16] OpenStreetMap contributors. (2024) OpenStreetMap. [Online]. Available: https://www.openstreetmap.org

[17] Panel on Frequency Allocations and Spectrum Protection for Scientific Uses, *Handbook of frequency allocations and spectrum protection for scientific uses*. National Academies of Sciences Engineering and Medicine and others, 2015.

[18] *Study on channel model for frequencies from 0.5 to 100 GHz*, 3GPP Technical Report 38.901, Nov. 2020.

[19] N. Sidiropoulos, T. Davidson, and Z.-Q. Luo, "Transmit beamforming for physical-layer multicasting," *IEEE Trans. Signal Process.*, vol. 54, no. 6, pp. 2239–2251, Jun. 2006.

[20] M. Grant and S. Boyd. (2014, Mar.) CVX: Matlab software for disciplined convex programming, version 2.1. [Online]. Available: https://cvxr.com/cvx

[21] ——, "Graph implementations for nonsmooth convex programs," in *Recent Advances in Learning and Control*. Springer-Verlag Limited, 2008, pp. 95–110.

[22] S. Kasdorf, B. Troksa, C. Key, J. Harmon, and B. M. Notaroš, "Advancing accuracy of shooting and bouncing rays method for ray-tracing propagation modeling based on novel approaches to ray cone angle calculation," *IEEE Trans. Antennas Propag.*, vol. 69, no. 8, pp. 4808–4815, Aug. 2021.

[23] Ettus Research. (2024) X300/X310 - Ettus Knowledge Base. [Online]. Available: https://kb.ettus.com/X300/X310

[24] ——. (2024) B200/B210/B200mini/B205mini - Ettus Knowledge Base. [Online]. Available: https://kb.ettus.com/B200/B210/B200mini/B205mini

[25] S. Munira, D. Saha, G. Hellbourg, and A. Dutta, "Dynamic protection zone for radio astronomy," in *IEEE Int. Symp. Dynamic Spectr. Access Netw.*, May 2024, pp. 556–560.
[26] S. Tschimben, A. Aradhya, G. Weihe, M. Lofquist, A. Pollak, W. Farah, D. DeBoer, and K. Gifford, "Testbed for radio astronomy interference characterization and spectrum sharing research," in *IEEE Aerospace Conference*, Mar. 2023, pp. 1–16.
[27] A. Sarbhai, F. Mitchell, S. Kasera, A. Bhaskara, J. Van der Merwe, and N. Patwari, "Reactive spectrum sharing with radio dynamic zones," in *IEEE Int. Symp. Dynamic Spectr. Access Netw.*, May 2024, pp. 429–438.
[28] J. Breen, A. Buffmire, J. Duerig, K. Dutt, E. Eide, M. Hibler, D. Johnson, S. K. Kasera, E. Lewis, D. Maas, A. Orange, N. Patwari, D. Reading, R. Ricci, D. Schurig, L. B. Stoller, J. Van der Merwe, K. Webb, and G. Wong, "POWDER: Platform for open wireless data-driven experimental research," in *Proceedings of the 14th International Workshop on Wireless Network Testbeds, Experimental Evaluation & Characterization*, Sep. 2020, p. 17–24.
[29] Y. Dai and H. Minn, "A spectrum sharing paradigm for gso satellite system and radio astronomy system," *IEEE Access*, vol. 7, pp. 93 952–93 973, Jul. 2019.
[30] X. Wei, A. Gupta, A. Dutta, D. Saha, and G. Hellbourg, "Ris for signal cancellation in 3d," in *IEEE Int. Symp. Dynamic Spectr. Access Netw.*, May 2024, pp. 412–419.
[31] S. Chakraborty, D. Saha, A. Dutta, and G. Hellbourg, "LOCI: Learning low overhead collaborative interference cancellation for radio astronomy," in *IEEE Int. Conf. Commun.*, May 2023, pp. 6391–6396.

Siddharth Dongre (Graduate Student Member, IEEE) completed the M.S. degree in Computing Security from Rochester Institute of Technology (RIT) in 2020. He received the Bachelor of Engineering degree in Computer Engineering from Pune University, India in 2017. He is currently pursuing a Ph.D. degree in Electrical and Computer Engineering at RIT. His research interests include secure spectrum sharing in 5G, Wi-Fi, and radio astronomy services; beamforming in MIMO systems; and vehicle-to-vehicle (V2V) communications security.

Tiep M. Hoang received the Ph.D. degree in Electronics, Electrical Engineering and Computer Science from Queen's University Belfast, United Kingdom, in 2019, the M.Eng. degree in Electronics and Radio Engineering from Kyung Hee University, South Korea, in 2014, and the B.Eng. degree in Electronics and Electrical Engineering from the HCMC University of Technology, Vietnam, in 2012. From 2020 to 2022, he was a Postdoctoral Fellow with the School of Electronics and Computer Science, the University of Southampton, United Kingdom. From 5/2022 to 8/2023, he was a Postdoctoral Fellow with the Department of Electrical Engineering, the University of Colorado Denver, United States. He is currently a Postdoctoral Fellow with the Department of Electrical and Microelectronic Engineering, Rochester Institute of Technology, United States. His research interests include 5G/6G wireless communications, physical-layer security and authentication, reconfigurable intelligent surface, convex optimization, and machine learning.

Hanif Rahbari (Member, IEEE) received the Ph.D. degree in electrical and computer engineering from the University of Arizona in 2016. He is currently an Associate Professor with the Golisano College of Computing and Information Sciences, and is affiliated with the ESL Global Cybersecurity Institute and Kate Gleason College of Engineering, Rochester Institute of Technology (RIT), NY. In Spring 2018, he joined RIT after an interim experience as a post-doctoral associate with Virginia Tech. He is also a co-inventor on three U.S. patents. His broad research interests include wireless ecosystem security and wireless communications, with an emphasis on jamming and privacy (transmission obfuscation) at the physical layer, connected vehicles security, applied (post-quantum) cryptography in wireless systems, and spectrum sharing security. He received the NSF CAREER Award in 2023.

Alireza Vahid (Senior Member, IEEE) received the B.Sc. degree in electrical engineering from Sharif University of Technology, Tehran, Iran, in 2009, and the M.Sc. and Ph.D. degrees in electrical and computer engineering from Cornell University, Ithaca, NY, USA, in 2012 and 2015 respectively. From 2015 to 2017, he worked as a postdoctoral research scientist at the Information Initiative at Duke University, Durham, NC, USA. From 2017 to 2023, he was an Assistant Professor of electrical engineering at the University of Colorado at Denver, Denver, CO, USA. He is currently a Gleason Endowed Associate Professor of Electrical and Microelectronic Engineering at Rochester Institute of Technology, Rochester, NY, USA. His research interests include network information theory, wireless communications, and applications of coding theory in high-performance computer memory systems. He received the 2015 Outstanding Ph.D. Thesis Research Award, the 2010 Director92s Ph.D. Teaching Award, Jacobs Scholar Fellowship in 2009 from Cornell University, the 2013 Qualcomm Innovation Fellowship, the 2019 Lab Venture Challenge Award, and the 2021 SONY Faculty Innovation Award. He currently serves as an associate editor for IEEE Communications Letters and IEEE Transactions on Information Theory.